

# Impact Fracture Behavior of Continuous Glass Fiber-Reinforced Nylon 6

J. U. OTAIGBE\* and W. G. HARLAND, *Department of Polymer Science and Technology, UMIST, Box 88, Manchester M60 1QD, England*

## Synopsis

The impact fracture toughness of nylon 6/continuous glass fiber composites at four levels of fiber content has been studied. The composites were produced by anionically polymerizing caprolactam within a glass mat using a vacuum injection technique. Application of linear elastic fracture mechanics to characterize the impact fracture toughness of the composites, using an energy approach ( $G_{IC}$ ), has been found to be applicable provided that a correction is made for the size of the damage zone. The concept of  $J_c$ , fracture energy per unit ligament area, has also been applied to the composites and agreement between  $G_{IC}$  and  $J_c$  has been found to be reasonably satisfactory. The ratio of crack propagation energy to the total energy absorbed (ductility index) has also been calculated. The ductility index was found to be close to one for the composites, indicating that additional energy is involved in propagating the fracturing cracks probably due to fiber debonding and/or crack blunting and fiber pullout. Fractographic examination of the impact fracture surface confirmed the presence of these features.

## INTRODUCTION

The automobile industry presents a great challenge to the plastics industry, particularly in terms of large-area moldings for car bodies. A satisfactory solution to this problem would result in an enormous increase in consumption of polymeric materials and in materials both fibrous and particulate used for reinforcement. The requirements of composites of these materials are well known to be strength, toughness to resist impact failure, and ability to absorb impact energy even with failure, high stiffness, resistance to fatigue, all combined with light weight relative to steel, for instance. Consequently, the detailed mechanical behavior of such materials is an important area of interest.

Impact behavior of such material is of paramount importance. Several investigators<sup>1-5</sup> have recently attempted to explain the fracture process in polymers using a fracture mechanics approach based on the Griffith criterion for unstable crack propagation.<sup>6</sup> They have evaluated a parameter,  $G_{IC}$  (called the critical strain energy release rate), which is a material property and is a measure of the fracture toughness of materials. Results obtained from fracture mechanics analyses have thrown considerable light upon the behavior of pure polymers under impact loading conditions. Presently, there is only a limited amount of published information on the relationships between frac-

\*To whom correspondence should be addressed: Department of Chemistry, University of Benin, Benin City, Nigeria.

ture toughness and composition in polymer composites, but a coherent picture is beginning to emerge as the subject develops. Extensive yielding and/or debonding usually precedes fracture in fiber-reinforced composites even in the presence of a sharp crack, so that linear elastic fracture mechanics techniques are unsuitable. However, a crack length correction factor that accounts for the plastic yielding and/or debonding observed in polymer composites has been applied to the analysis of the fracture data of these materials by other workers.<sup>2,7,8</sup> Because of the difficulties associated with the determination of a correction factor, it is sometimes advocated that the concept of  $J_c$ , fracture energy per unit ligament area, which represents the original fracture criteria, be used when full yielding occurs.<sup>2</sup>

This work is aimed particularly at establishing the physical and fracture characteristics of the behavior of planar-random continuous glass (swirl) mat-reinforced nylon 6 under impact loading condition. A falling dart system with an instrumented tup has been used to give force-time data and the fracture mechanics approach (in energy terms) used to interpret the results. The material property,  $G_{IC}$ , has been evaluated for all the materials. The fracture energy per unit ligament area,  $J_c$ , was also calculated for the composites and the micromechanisms of energy absorption examined using scanning electron and optical microscopy.

## EXPERIMENTAL

The composites were produced in the form of plates (4-mm thick) by polymerizing caprolactam in situ within a mat of swirl-type continuous glass fiber compressed to the final thickness of composite required and containing the required volume fraction of glass fiber. The fibers had an average diameter of 15  $\mu\text{m}$  and a tex (weight in grams of one kilometer of fiber) of 25. The products were isotropic in the plane of the plate. The glass mat was heat-cleaned before use because it was observed that the size (coupling agent) on the glass fibers greatly inhibited the polymerization reaction. Sheets of nylon 6 were prepared in a similar manner. A more detailed description of the fabrication technique is given elsewhere.<sup>9,10</sup>

An instrumented falling weight impact tester, described elsewhere,<sup>10,11</sup> was used to carry out the tests on nylon 6 and composites using an average striker velocity of 4  $\text{ms}^{-1}$ . Measurements were made on materials with volume fractions of glass fiber zero, 0.17, 0.22, 0.26, and 0.33. Rectangular beam specimens with smoothed edges were cut from the molded plates, and notches of various lengths up to 40% of the width  $D$  were milled at the center of the specimen using a V-shaped cutter. To ensure ideal sharp conditions the notches were sharpened with a razor blade prior to testing. At least 5 specimens, dried to constant weight, were tested at room temperature at each notch depth. The notch depth of the broken half of each specimen was measured using a traveling microscope. The ratio of span length to specimen width or depth,  $S/D$ , was maintained at 4 throughout the tests.

The load was scaled directly from the oscilloscope photograph, while the energy required a kinetic energy correction<sup>11</sup> due to the change in the velocity of the tup during the impact. The energy could be determined at any stage of the test. The most significant cracking occurred at the peak load when the

initiation energy,  $W_I^*$ , was added to the specimen. The rest of the fracture energy,  $W_p^*$ , was used to propagate the crack(s) until ultimate failure occurred. The total energy,  $W_T^*$ , is the sum of  $W_I^*$  and  $W_p^*$ .

A microscopic study of the fracture surfaces was carried out using optical and scanning electron microscopy. In the former technique specimen sections local to the fracture surface were cut and cast in acrylic resin, polished on metallographic wheels with increasingly fine abrasives. The polished surface was then viewed in an optical microscope with a camera attached. The latter technique did not require any special techniques except that the samples were coated with gold in order to render them conductive.

### Analysis of Test Results

The experimental data obtained from the tests were analyzed in energy terms using linear elastic fracture mechanics techniques.<sup>1,2</sup> The critical strain energy release rate,  $G_{IC}$ , was calculated from the following equation:<sup>1,2</sup>

$$W_I^* = G_{IC}BD\phi \quad (1)$$

$W_I^*$  is the crack initiation energy,  $B$  is the specimen thickness, and  $D$  is the specimen width or depth.  $\phi$  is a geometrical correction factor determined as a function of  $a/D$  where  $a$  is the original crack length.<sup>2</sup> Equation (1) implies that a plot of  $W_I^*$  versus  $BD\phi$  should give a straight line passing through the origin and with slope  $G_{IC}$ .<sup>1</sup> The critical strain energy release rate  $G_{IC}$ , is often reported in the literature as  $G_c$ , the "I" being dropped for convenience.

The possibility of plastic yielding and/or debonding taking place either at the crack-tip region or in net section of the specimen must be considered. If yielding is confined to the crack-tip region, linear elastic fracture mechanics can be used if the crack length is modified to take into account the plastic or damage zone length.<sup>2,7,8,12</sup> The modified crack length,  $a_f$ , used in the calculation of  $G_{IC}$  is given by  $a_f = a + r_d$ , where  $r_d$  is the plastic or damage zone length. Since the correction factor  $r_d$  involves  $G_{IC}$ ,<sup>2,13</sup> an iterative procedure is required, but convergence occurs rapidly. To overcome this difficulty, the concept of  $J_c$ , fracture energy per unit ligament area, is applied when full yielding occurs.<sup>2</sup> This is defined such that  $J_c = G_{IC}$  for the elastic case, but it is applicable for all degrees of plasticity and is given by:<sup>2</sup>

$$J_c = \frac{2W_T^*}{A} \quad (2)$$

where  $A = B(D - a)$  = cross-sectional area of the fractured ligament. The factor 2 in Eq. (2) arises because the average crack tip displacement in bending is one-half the crack tip displacement in tension.<sup>2</sup> Both Eqs. (1) and (2) were used to analyze the experimental data.

The total energy absorbed in the fracture process,  $W_T^*$ , is a combination of two energy terms, namely, the crack initiation and propagation energies (i.e.,  $W_I^*$  and  $W_p^*$ , respectively). The former is the energy absorbed at maximum load and  $W_p^*$  is the total energy absorbed less  $W_I^*$ . By nondimensionalizing this total energy relationship, the informative ratio  $W_p^*/W_T^*$ , called here the

ductility index (DI), was calculated for specimens with  $a/D$  of 0.4. The DI as defined above varies between zero (brittle fracture) and unity (gross yielding).

## RESULTS AND DISCUSSION

Representative impact load-time curves for nylon 6 and a composite ( $V_f = 0.33$ ) are shown in Figures 1 and 2, respectively. It can be seen from these figures that time to fracture and total energy required to fracture the specimen varies with notch depth. The load-time curve for the unreinforced nylon 6 (Fig. 1) is typical of a brittle failure with the peak load clearly defined and returning to the baseline at the fracture point. The negative load and the jagged section of the load line after specimen failure (Fig. 1) is believed to be due to inertial effects such as vibrations inside the strain gaged tup.<sup>11</sup> This region of the load-time curves is easily detected and rejected in the computer analysis of the impact data. For this material the crack propagation energy,  $W_p^*$ , is negligibly small compared to  $W_I^*$ . The load-time curves for the composites (Fig. 2) are complex in nature showing double peaks at the maximum load and multiple peaks between maximum load and complete fracture. The double maximum peaks observed are characteristic of pseudo-ductile materials (e.g., metals and continuous fiber-reinforced plastics).<sup>7,14</sup> For these materials the total energy absorbed in the fracture process is a combina-

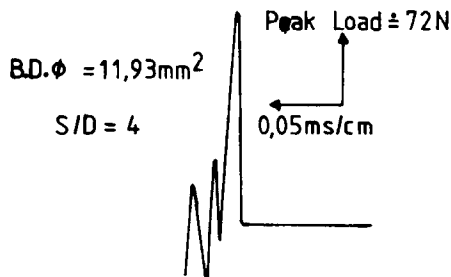
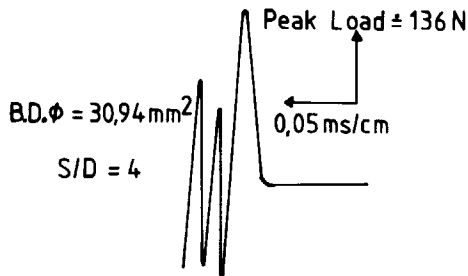


Fig. 1. Impact load-time curve for pure nylon 6 matrix with values of  $S/D$  and  $BD\phi$  as shown.

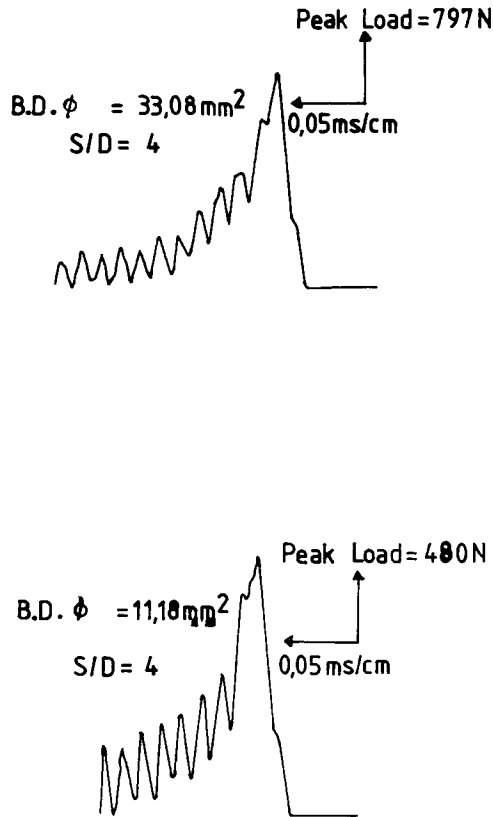


Fig. 2. Impact load-time curve for composite of ( $V_f = 0.33$ ) with values of  $S/D$  and  $BD\phi$  as shown.

tion of the crack initiation energy ( $W_I^*$ ) and  $W_p^*$ . As mentioned earlier, the former is the energy absorbed at maximum load and  $W_p^*$  is the total energy absorbed less  $W_I^*$ . The additional peaks in the load-time curves of the composites (Fig. 2) are due to vibrations in the loading system and/or flexural vibrations in the specimen.

Using Eq. (1), it was possible to evaluate  $G_{IC}$  for the specimens by plotting  $W_I^*$  versus  $BD\phi$ . Typical plots of corrected  $W_I^*$  versus  $BD\phi$  for nylon 6 and a composite ( $V_f = 0.33$ ) are shown in Figures 3 and 4, respectively. Corresponding plots for composites with intermediate fiber volume fractions are similar to these plots. However, kinetic energy loss and stress waves in the specimen after fracture results in a positive intercept in the plot.<sup>1,2</sup> This intercept was subtracted from the measured  $W_I^*$  values, thus yielding a straight line passing through the origin.<sup>1,2,11,13</sup> The use of several notch depths means that  $G_{IC}$  is determined from the slope of the data, which eliminates the intercept effect from the result. The scatter in the data is typical of impact testing and the best straight line through the points was drawn using the least squares method.

It has been shown by other workers that randomly oriented chopped-strand mat-reinforced plastics required a correction for the debonded zone size before

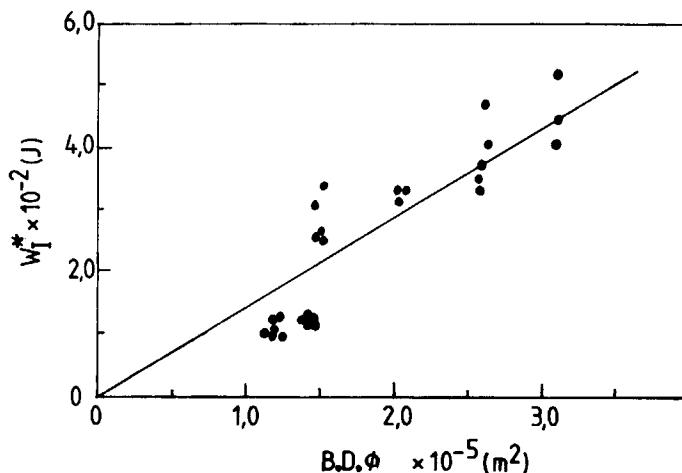


Fig. 3. Corrected crack initiation energy,  $W_I^*$ , versus  $BD\phi$  for pure nylon 6 matrix.

the fracture toughness,  $K_{IC}$  and hence  $G_{IC}$ , behaved as material properties.<sup>7,15</sup> This correction was carried out for the composites used in this study by means of a computer program and a correction of 1.0 mm was found to be suitable, and gave  $G_{IC}$  values with correlation coefficient better than 0.96 for all the specimens.

The concept of fracture energy per unit ligament area,  $J_c$ , is frequently used to analyze the fracture data of materials showing gross plastic yielding with high energy absorption due to the difficulties associated with the determination of a correction factor for plastic yielding. Using Eq. (2), it was possible to evaluate  $J_c$  by plotting  $W_I^*$  versus  $B(D - a)$  for the composites. Figures 5 and 6 show typical  $W_I^*$  versus  $B(D - a)$  plots, with the intercept subtracted for composites with  $V_f = 0.17$  and 0.33, respectively. These plots give reasonable lines through the origin, as expected from Eq. (2), except for the smallest

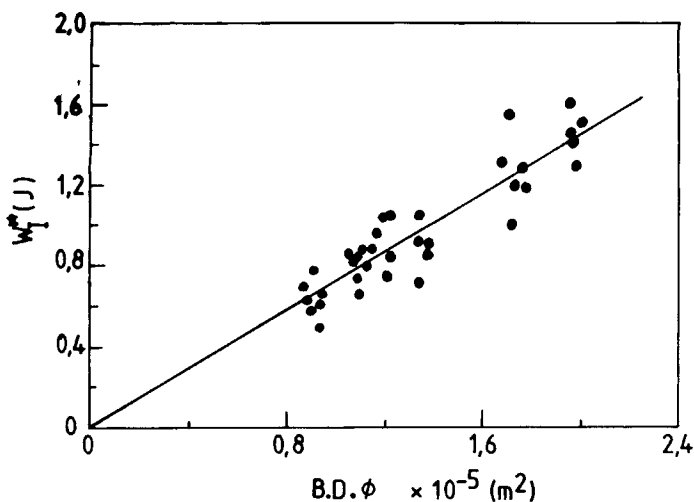


Fig. 4. Corrected crack initiation energy,  $W_I^*$ , versus  $BD\phi$  for composite of  $V_f = 0.33$ .

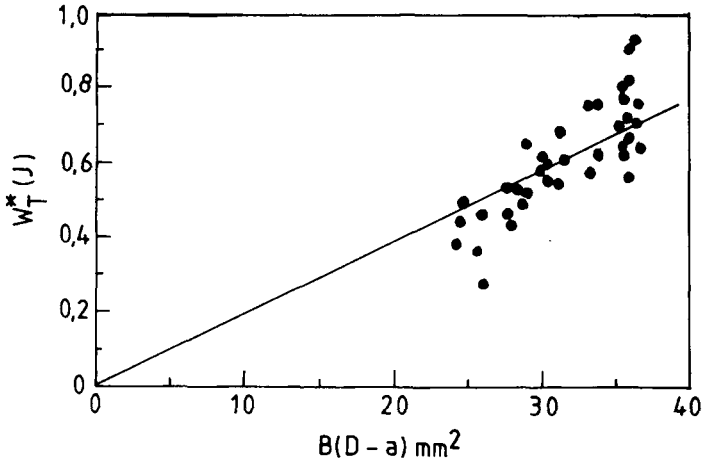


Fig. 5. Corrected total absorbed energy,  $W_T^*$ , versus fractured ligament area,  $B(D-a)$ , for composite of  $V_f = 0.17$ .

notch depths where there is some divergence. The best straight line was drawn through the points using the least-squares methods as before. Corresponding plots for composites with fiber volume fractions, 0.22 and 0.26, are similar to the above plots. The  $G_{IC}$  and  $J_c$  values obtained for all the materials are shown in Figure 7. The agreement between  $G_{IC}$  and  $J_c$  is good. Figure 7 shows that the variation of  $G_{IC}$  and  $J_c$  with fiber volume fraction is nonlinear and a dramatic improvement in the fracture parameters of nylon 6 matrix is obtained when it is reinforced with heat-cleaned continuous glass fibers. Similar trends of results are reported elsewhere for continuous glass fiber-reinforced polypropylene.<sup>16</sup>  $G_{IC}$  obtained for the pure nylon 6 matrix,  $1.40 \text{ kJm}^{-2}$ , is within the range reported for a similar polymer, nylon 66,  $0.25\text{--}4.0 \text{ kJm}^{-2}$ .<sup>17</sup> Phang,<sup>18</sup> obtained a value of  $1.92 \text{ kJm}^{-2}$  for impact  $G_{IC}$  for nylon 66.  $G_{IC}$  obtained for the composites, used here, varies from  $43\text{--}72 \text{ kJm}^{-2}$  depending on

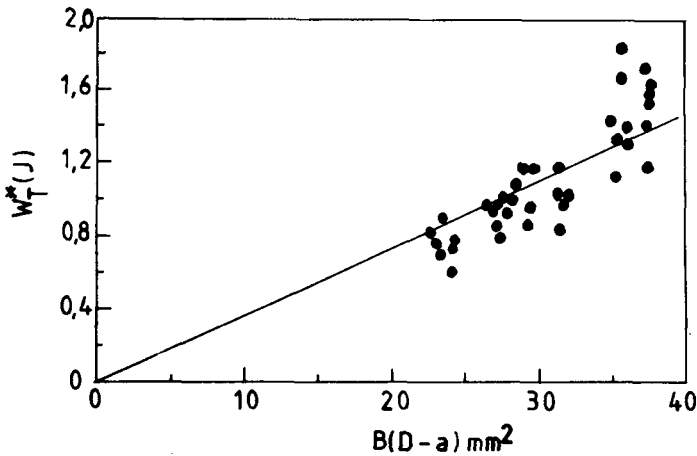


Fig. 6. Corrected total absorbed energy,  $W_T^*$ , versus fractured ligament area,  $B(D-a)$ , for composite of  $V_f = 0.33$ .

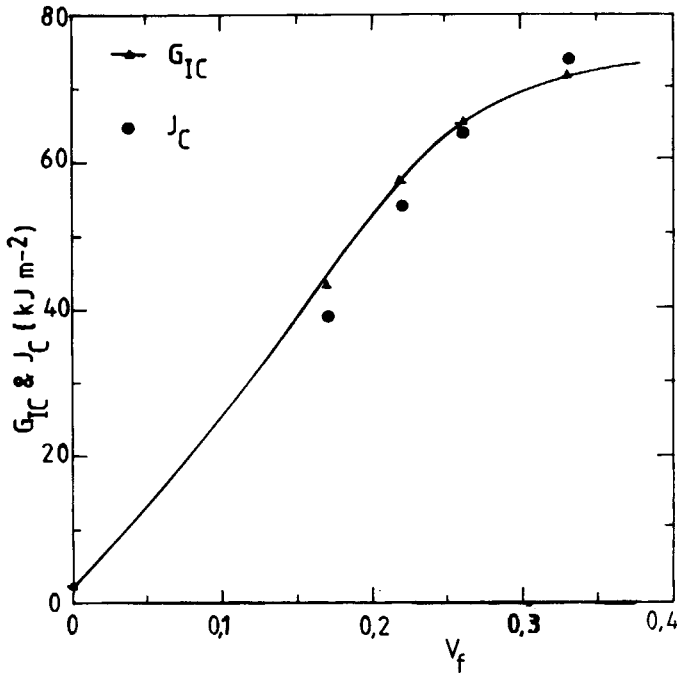


Fig. 7. Variation of  $G_{IC}$  ( $\Delta$ ) with  $V_f$  for nylon 6 and composites. ( $\bullet$ )  $J_C$ .

the level of reinforcement. This is comparable to chopped strand mat-reinforced polyester with impact energies in the range 50–80  $\text{kJm}^{-2}$ , where the pure polyester matrix has a typical impact energy of 2  $\text{kJm}^{-2}$ .<sup>19</sup> However the  $G_{IC}$  values obtained for the present composites are much higher than the  $G_{IC}$  value of 12.0  $\text{kJm}^{-2}$  for short-fiber-reinforced nylon 66 ( $V_f = 0.23$ ).<sup>18</sup>

The DI for the nylon 6 and composites are shown in Figure 8. A DI close to zero implies that most of the total absorbed energy,  $W_T^*$ , is absorbed before

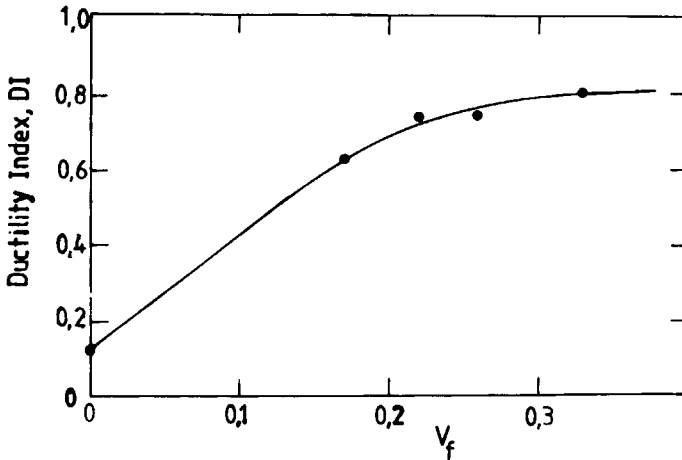


Fig. 8. Average ductility index, DI, versus volume fraction for specimens with  $a/D = 0.4$ .



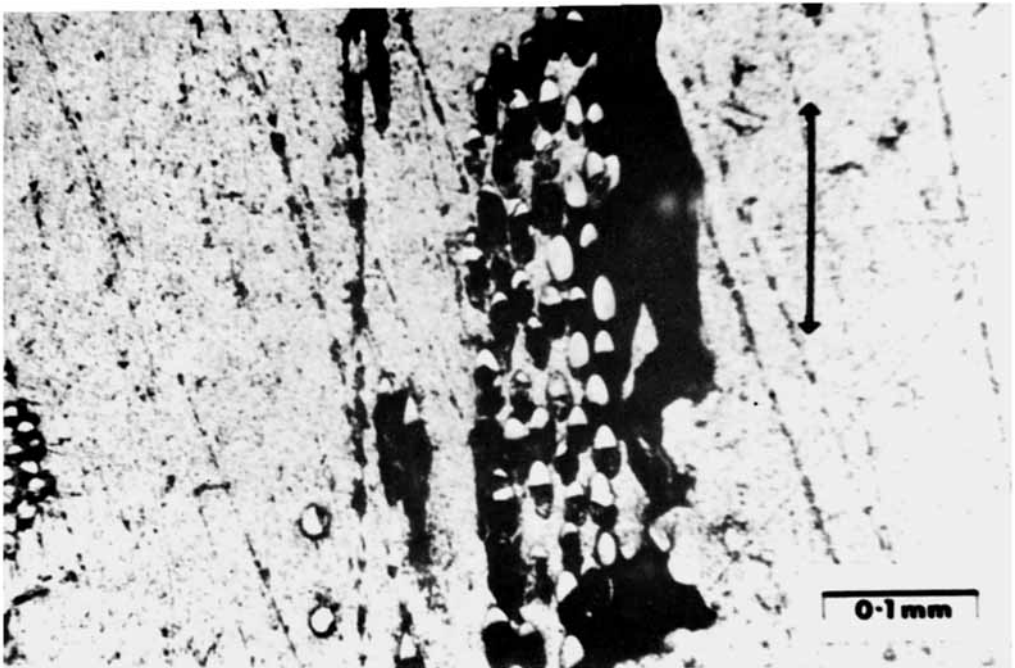


Fig. 9. Cross-section close to the notch tip of impact fracture surface showing fiber splitting and/or debonding ( $\leftrightarrow$  direction of crack propagation).

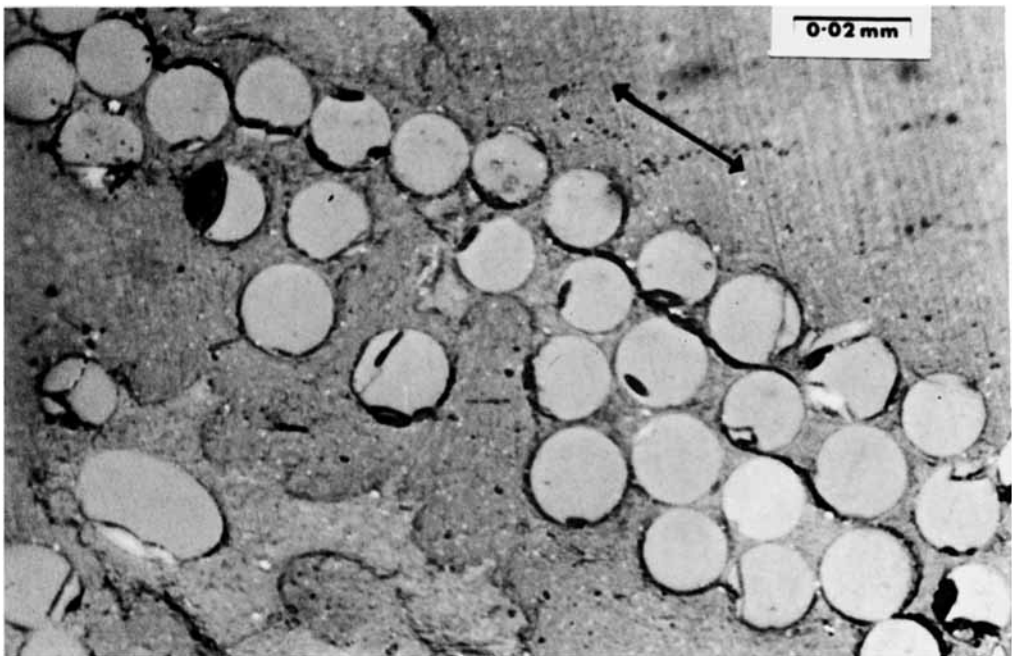


Fig. 10. Cross-section close to the notch tip of impact fracture surface showing crack propagation parallel to fibers ( $\leftrightarrow$  direction of crack propagation).

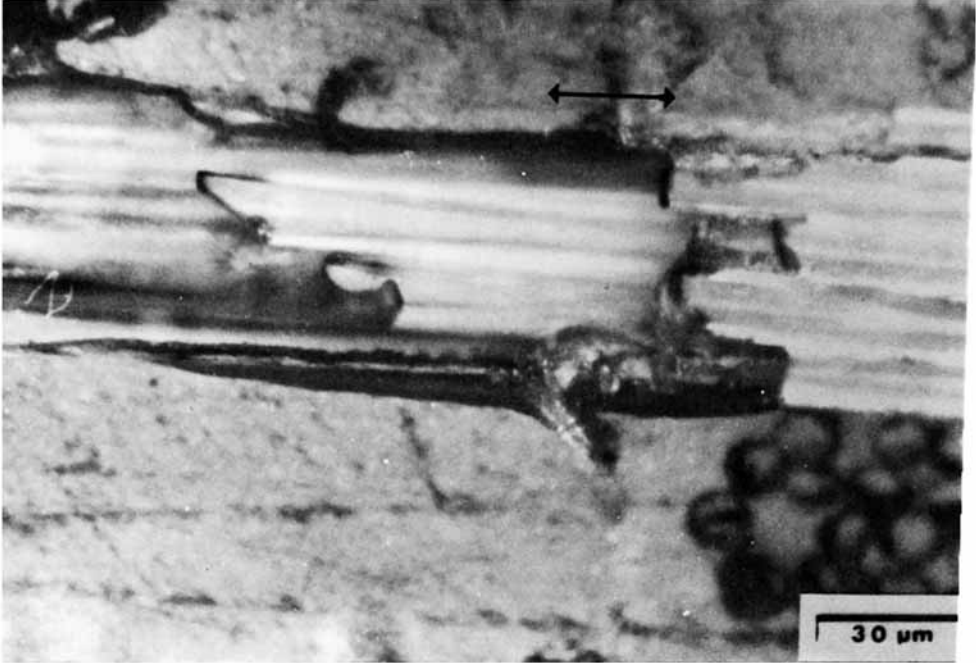


Fig. 11. Cross-section close to the notch tip of impact fracture surface showing fiber failures and pullout ( $\leftrightarrow$  direction of crack propagation).



Fig. 12. SEM of impact fracture surface showing extent of fiber pullout.

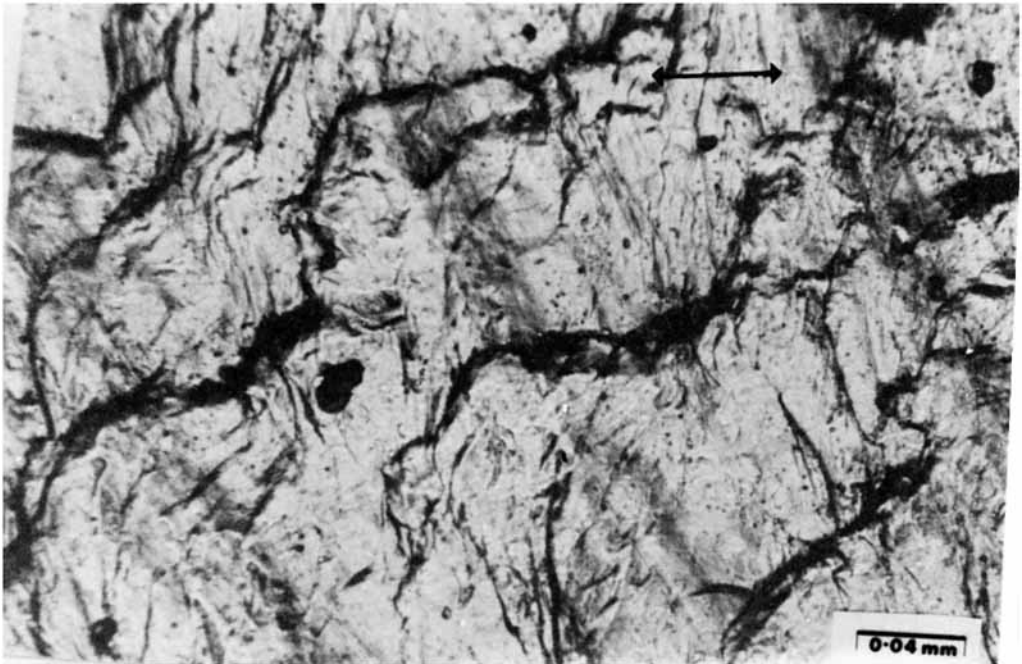


Fig. 13. Cross-section close to the notch-tip of impact fracture surface ( $V_f = 0.0$ ) showing cracks advancing smoothly and regions of crack initiation ( $\leftrightarrow$  direction of crack propagation).

the ultimate crack is initiated.<sup>14</sup> The closer DI is to unity, the larger the share of the total absorbed energy used to complete the failure after the peak load. It is evident from Figure 8 that the minimum DI was obtained for specimens with  $V_f = 0.0$  and the largest for specimens with  $V_f = 0.33$ . This ductility index behavior is probably due to the fiber failure and pullout and fibers debonding ahead of the growing crack. Evidence for the above behavior was found on examination of the fractured surfaces of the test specimens (Figs. 9–12). The observed ductility index behavior can be explained by considering the crack propagation phenomena. Continuous fiber at the tip of the crack, prior to fracture, may debond and blunt, stop or redirect the crack parallel to the fibers (Figs. 9 and 10), thus altering the stresses at the crack tip. The fibers can also fail at their weakest point and pullout (Fig. 11), thus working against frictional sliding.<sup>7</sup> Figure 13 shows cracks advancing smoothly through the cross-section of the pure nylon 6 matrix and conical markings that are associated with the interaction of the primary crack front with secondary cracks forming ahead of the main crack front.<sup>8,20</sup> These features are commonly associated with unstable crack propagation exhibited by brittle materials. In the examination of the surfaces of the fractured specimens, no matrix cracks were observed for the composites, all the cracks tended to occur at interfaces especially in regions of high fiber density (Figs. 9 and 10). The micrographs show that the fiber–matrix bond is weak, which is advantageous for resistance to impact failure of continuous fiber-reinforced composites.

## CONCLUSIONS

It has been shown that the impact fracture properties of swirl mat-reinforced nylon 6 may be explained using linear elastic fracture mechanics theory (in energy terms), provided that a correction is made for the size of the damage zone, which would otherwise invalidate the applicability of the above theory. Incorporation of heat-cleaned swirl type glass mat reinforcement in nylon 6 led to a dramatic improvement in the fracture parameters of the pure matrix.

The results obtained suggest that more than one type of toughening mechanism is responsible for the fracture process. The more usual and desirable composite situation is where an advancing crack does not break the fiber immediately, but may be left bridging the crack (as in the present composite system), and gives a pseudoductile behavior to a composite system containing brittle components.

## NOMENCLATURE

$a$	notch or crack length
$B$	specimen thickness
$D$	specimen depth or width
DI	ductility index
$G_{IC}$	critical strain energy release rate
$J_c$	fracture energy per unit ligament area
$\phi$	geometrical function determined as a function of $a/D$
$r_d$	plastic or debonding zone length
$S$	span length
$W_T^*$	total energy absorbed in fracture
$W_I^*$	crack initiation energy
$W_p^*$	crack propagation energy

The authors are grateful to Dr. J. P. Berry (UMIST) England for his useful comments and criticisms. The scholarship award to J. U. O. by the University of Benin toward a Ph.D degree, and the assistance of Mr. A Appleyard (UMIST) for the computer treatment of the experimental data are gratefully acknowledged.

## References

1. G. P. Marshall, J. G. Williams, and C. E. Turner, *J. Mater. Sci.*, **8**, 949 (1973).
2. E. Plati and J. G. Williams, *Polym. Eng. Sci.*, **15**, 470 (1975).
3. P. L. Fernando and J. G. Williams, *Polym. Eng. Sci.*, **20**, 3 (1980).
4. P. L. Fernando and J. G. Williams, *Polym. Eng. Sci.*, **21**, 15 (1981).
5. J. G. Williams, *Adv. Polym. Sci.*, **27**, 67 (1978).
6. A. Griffith, *Phil. Trans. R. Soc., Ser. A*, **221**, 163 (1920).
7. F. J. McGarry and J. F. Mandel, *Faraday Spec., Disc. Soc.*, **2**, 90 (1972).
8. M. J. Owen and R. G. Rose, *J. Phys. D: Appl. Phys.*, **6**, 42 (1973).
9. J. U. Otaigbe and W. G. Harland, *J. Appl. Polym. Sci.*, in press.
10. J. U. Otaigbe, Ph.D. thesis, University of Manchester, Manchester, England, June 1984.
11. D. R. Ireland, in *Instrumented Impact Testing*, ASTM STP 563, American Society for Testing and Materials, 1974, p. 3.

12. F. A. McIntook, *Fracture Testing of High Strength Sheet Materials*, Materials Research and Standards, Vol. 1, 1961.
13. J. G. Williams, *Fracture Mechanics of Polymers*, Ellis Horwood Ltd., Chichester, 1984, Chap. 8.
14. J. D. Helfinstine, in *Charpy Impact Energy of Unidirectional Graphite/Aramid/Epoxy Hybrid Composites*, Composite Materials: Testing and Design, 4th Conference, ASTM-STP 617, 1977, p. 375.
15. P. W. R. Beaumont and D. C. Phillips, *J. Mater. Sci.*, 7, 682 (1972).
16. J. H. Davis, *Plastics and Polymers*, 39, 137 (1971).
17. P. E. Reed, in *Developments in Polymer Fracture-1*, E. H. Andrew, ed., Applied Science Publishers Ltd., 1979, p. 121.
18. K. W. Phang, Ph.D. thesis, University of Manchester, Manchester, England, 1981.
19. R. J. Crawford, *Plastics Engineering*, Pergamon Press, Oxford, 1981, Chap. 3.
20. I. M. Ward, *Mechanical Properties of Solid Polymers*, Wiley-Interscience, London, 1971.

Received December 9, 1987

Accepted December 21, 1987